Voyager Orbit Determination at Jupiter

JAMES K. CAMPBELL, STEPHEN P. SYNNOTT, AND GERALD J. BIERMAN, SENIOR MEMBER, IEEE

Abstract—**This paper summarizes the Voyager 1 and Voyager 2 orbit determination activity extending from encounter minus 60 days to the Jupiter encounter, and includes quantitative results and conclusions derived from mission experience. The major topics covered include an identification and quantification of the major orbit determination error sources and a review of salient orbit determination results from encounter, with emphasis on the Jupiter approach phase orbit determination. Special attention is paid to the use of combined spacecraft-based optical observations and Earth-based radiometric observations to achieve accurate orbit determination during the Jupiter encounter approach phase.**

I. INTRODUCTION

ON March 5, 1979 after a journey of 546 days and slightly more than 1 billion km, the Voyager 1 spacecraft passed within 0.3 Jupiter radii of the innermost Galilean satellite Io. Four months later, on July 8, Voyager 2 flew by the third Galilean satellite Ganymede at 0.8 Jupiter radii, and then by Jupiter the next day, at 10 Jupiter radii. Fig. 1 shows the Voyager heliocentric trajectory, and Figs. 2 and 3 show the near Jupiter trajectory for each mission. These Voyager encounters with Jupiter proved to be both spectacular and historic, with each mission returning voluminous data from 11 scientific instruments, including some 15 000 high resolution pictures of Jupiter and five of its satellites. After passing Jupiter, both spacecraft flew on to Saturn. Voyager 1 had encounters with several Saturn satellites, including a close flyby of the massive satellite Titan, on November 12, 1980. Voyager 2 encountered Saturn and its satellites on August 26, 1981; this spacecraft has undertaken the long journey to Uranus and will encounter that planet in January 1986, providing the first closeup view of that planet and its satellites. If the spacecraft remains healthy, it will then embark on its fourth interplanetary cruise, arriving at the planet Neptune in 1989. The orbit determination discussed in this paper is confined to the Jupiter encounter phase.

The spacecraft flight path had to be accurately controlled to achieve its scientific objectives. Since the final trajectory correction maneuver and its associated execution errors were small, the Jupiter delivery accuracies were determined by the orbit estimation accuracies available at the time of maneuver specification. From postencounter reconstruction of each flyby trajectory it has been determined that the final orbit control was within the accuracy predicted by the filter/smoother covariance analyses. The accurate instrument sequences required to obtain the near encounter science data were highly dependent upon accurate postcontrol knowledge of the spacecraft trajectory and satellite orbits. The results from the reconstructed orbits indicate that the near encounter spacecraft orbits were predicted to within 50 km and that spacecraft-satellite pointing was predicted to within 3 mrad, even for the close (20 000 km) Voyager 1 Io flyby.

This paper briefly describes the navigational measurement system and error source modeling used to produce accurate Jupiter-relative orbit determination. We will focus

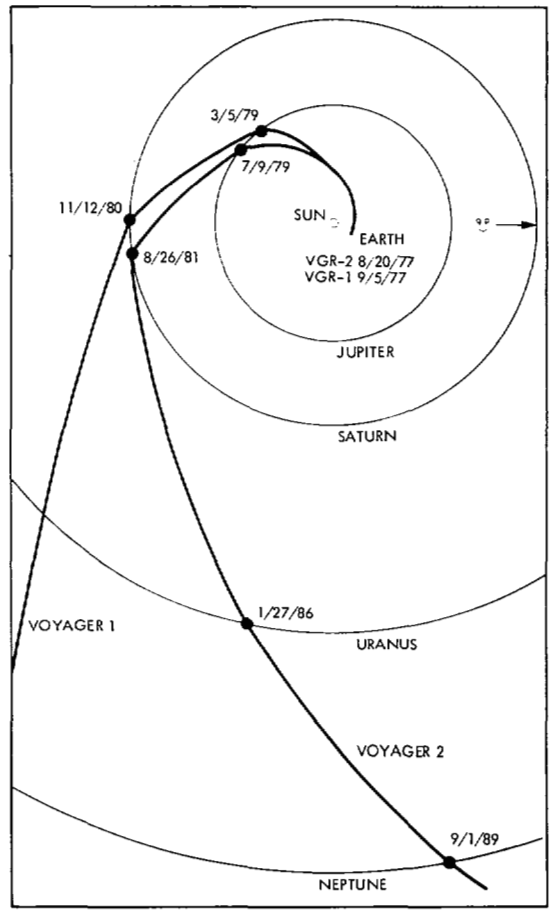

Fig. 1. Voyager 1 and 2 heliocentric trajectories.

Manuscript received March 5, 1982; revised September 7, 1982 and September 20, 1982. This work was supported by NASA under Contract NAS7-100 and Factorized Estimation Applications, Inc.

J. K. Campbell and S. P. Synnott are with the Jet Propulsion Laboratory, California Institute of Technology, Pasadena, CA 91109.

G. J. Bierman was with the Navigation Systems Section, Jet Propulsion Laboratory, California Institute of Technology, Pasadena, CA 91109. He is now with Factorized Estimation Applications, Inc., Canoga Park, CA 91307.

0018-9286/83/0300-0256$01.00

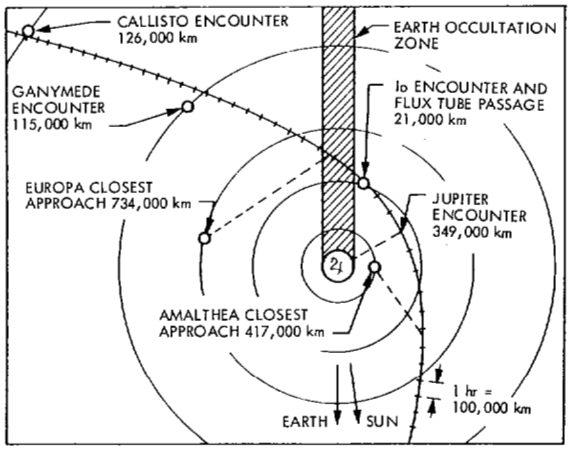

Fig. 2. Voyager 1 Jupiter flyby geometry.

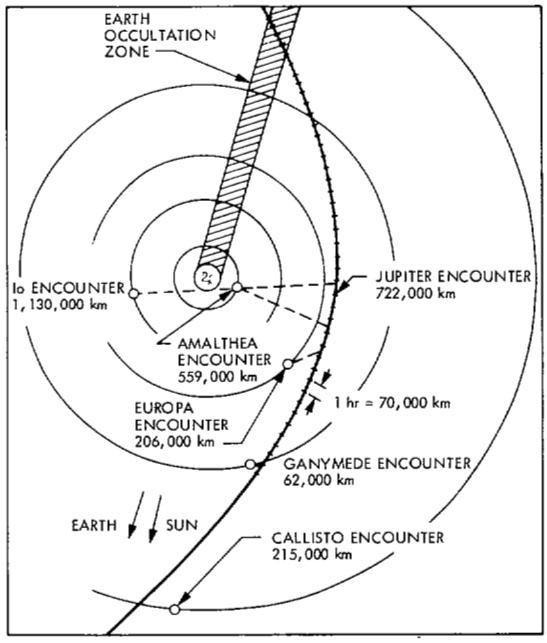

Fig. 3. Voyager 2 Jupiter flyby geometry.

on the particular problem of combining the orbit information content from two distinct sources; Earth-based radiometric observations (range and Doppler) and spacecraft-based optical observations to achieve accurate orbit determination during the planetary approach. Because this paper is an application of modern estimation, the reader is assumed to be familiar with the estimation concepts that are employed. The algorithmic formulations based on matrix factorization that are used to compute the orbit determination estimates, estimate error sensitivities, and estimate error covariances (filter/smoother and consider filter/smoother) are described (in great detail) in [1], [2], [6], and [7]. The latter part of Section II contains a discussion of the merits of the SRIF/SRIS and $U-D$ covariance factorized estimation algorithms that are used throughout this application.

The research reported here is extracted in large part from the Voyager navigation team report [8]. Interested readers are urged to consult this reference and also [10], which documents the Voyager Saturn encounter orbit determination.

II. Navigation Filter Design Rationale

There were two principal reasons for using a sequential stochastic filtering algorithm to process the Voyager tracking data. The first reason has to do with modeling of nongravitational accelerations and the second has to do with modeling of the optical data to account for pointing errors. Let us first focus on the nongravitational force problem.

The Voyager spacecraft, shown in Fig. 4, are three-axis stabilized vehicles, and remain in an Earth-pointed orientation relative to the Sun and a star, usually Canopus, for long periods of time. Notable features of the spacecraft are the large antenna dish, the science scan platform, and the groups of thrusters. The thrusters are unbalanced, since they do not fire in pairs, and are separated from the center of mass on opposite moment arms. A consequence of this configuration is that each time that a thruster is fired to either maintain or change the spacecraft attitude, there is a net translational velocity imparted to the spacecraft. Motion of the scan platform puts torque on the spacecraft, requiring thruster firings to maintain alignment. The effective center of solar pressure does not coincide with the spacecraft center of mass, and this can cause one-sided thruster firings.

A design flaw of the spacecraft is that the exhaust plumes from the positive and negative pitch attitude thrusters, which have velocity components along the radiometric measurement direction, strike the spacecraft structure. This fact was known before launch, but it was believed that the effect would be negligible. The conclusion of a postlaunch study was that, in fact, the plume impingement effect is significant.

Spacecraft outgassing as a byproduct of attitude control was considered to be basically a dynamic stochastic process which imparted ΔV velocity impulses to the spacecraft. The nature of these pulses was such that over a daily period the net translational effect on the spacecraft was zero. However, the Doppler tracking data were significantly corrupted by this attitude control pulsing. It has been known for some time [9] that estimate accuracy severely degrades when such disturbances are not accounted for in the filter model, and it was demonstrated early in the flight that the OD estimates produced from radiometric data without taking into account a dynamic stochastic process propagated poorly and gave inaccurate orbit predictions. Doppler residuals could be more accurately predicted from a previous fit which assumed a stochastic process than from a fit to the same data where stochastic effects were ignored.

These spacecraft generated forces are commonly termed spacecraft nongravitational forces. For Voyager, small attitude control impulses were averaged over a daily period and treated as piecewise constant stochastic accelerations

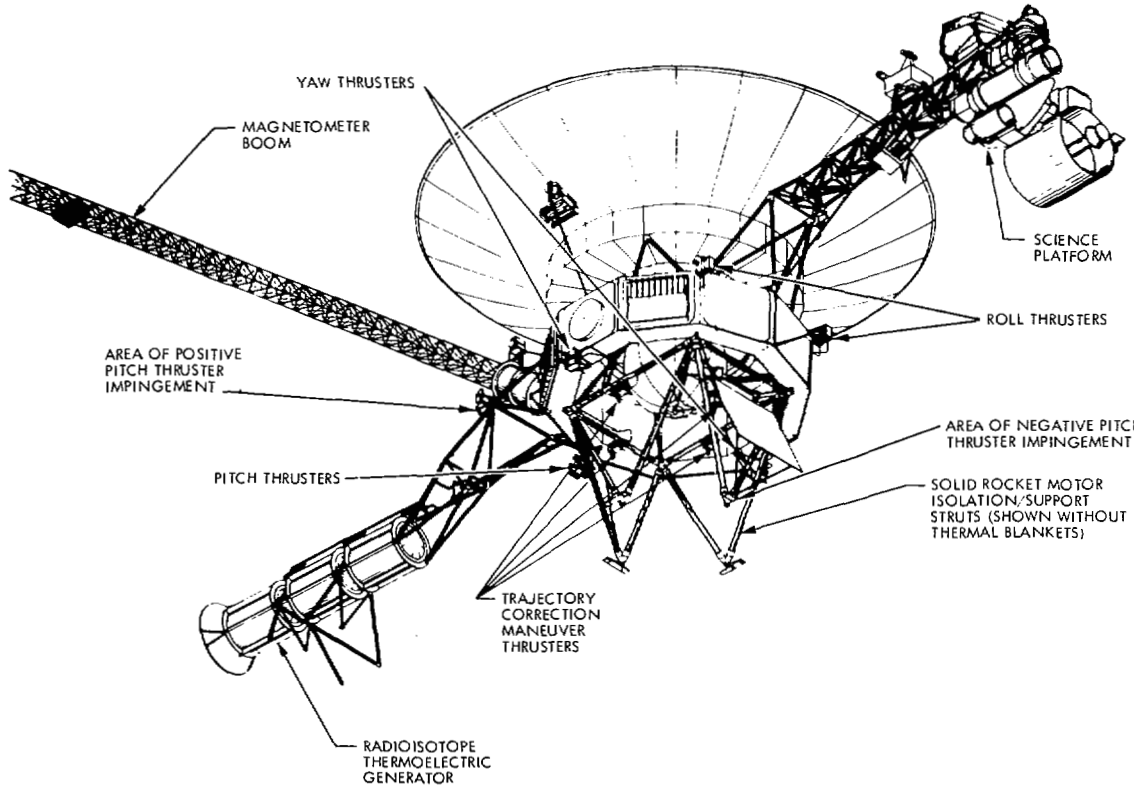

Fig. 4. Voyager spacecraft configuration.

along the respective spacecraft axes. Short term larger magnitude velocity impulses resulting from spacecraft turns were explicitly modeled as velocity impulses and were included in the list of parameters to be solved for (see Table I). Because of observability considerations, the stochastic effect was only significant in the axis which was aligned with the Doppler measurement direction, i.e., the Earth-spacecraft direction. Being able to eliminate unnecessary filter model state variables was doubly important because storage limitations imposed by the JPL Voyager ODP allows at most 70 parameters to be included in the filter model and, as a perusal of Table I shows, there are a considerable number of items to be estimated.

Let us turn attention now to the second reason for utilizing a sequential stochastic model, which has to do with the processing of optical measurements. These approach measurements were required to allow accurate orbit control at the final approach maneuver time. Doppler measurements which are sufficiently sensitive to Jupiter's gravity to allow determination of accurate planet-relative orbits occur too late for the information to be used for the final control maneuvers.

The optical data consisted of about 95 pictures processed for Voyager 1, and 113 pictures processed for Voyager 2. Galilean satellites (130 Voyager 1 satellite images, 143 Voyager 2 satellite images) were imaged against a star background with the narrow-angle imaging science instrument, which has a resolution of 10 μrad. The exposure time of the frames was 960 ms, sufficiently long to ensure the detection of dim stars up to a 9.5 effective visual magnitude. The optical data for orbit estimate solutions that are in agreement with the chosen Voyager 1 and 2 reconstruction solutions were fit to 0.25 pixels rms and essentially zero mean. No remaining systematic trends were detected *a posteriori*, indicating that there were no pixel level biases or center-finding errors inherent in the image extraction process.

The major navigational error source to be accounted for after extracting the star locations and satellite center locations is associated with inertial camera pointing. These errors were accounted for on a frame-by-frame basis, i.e., camera pointing errors were modeled as (frame dependent) white noise, and known inertial positions of the background stars in each frame were utilized. This type of stochastic model structure invites the use of a Kalman filter. Processing of these images produced accurate Jupiter-relative spacecraft orbit estimates that were used to construct the final control maneuvers. In addition, accurate satellite ephemerides were also determined [15] and these were used to define science instrument pointing.

Since this paper is a Kalman filter application, it is important to discuss the estimation processing techniques that were employed. It is a standard practice at JPL to implement navigation filters using square-root factorization techniques; even unweighted least-squares parameter fits are generally implemented using orthogonal transformation triangularization. Our experience with such things is that there are so many modeling and mission-related problems to worry about that we prefer to minimize numerical error effects as even a possible cause of poor

TABLE I
67 STATE VOYAGER NAVIGATION MODEL WITH ESTIMATION RESULTS BASED ON ENCOUNTER DATA FROM FEBRUARY 9–MARCH 18, 1979

State	A Priori Sigma	A Posteriori (smoothed sigmas)	Remarks
Cartesian positions (3)	500.0 km	88.0 km	Smoothed values are RMS over the 108-step time arc.
Cartesian velocities (3)	.5 m/s	0.06 m/s	
Line-of-sight (s/c - Earth) non-gravitational accelerations			
bias (1)	5.0×10^{-12} km/s^2	1.5×10^{-12} km/s^2	
piecewise constant random (1)	5.0×10^{-12} km/s^2	2.5×10^{-12} km/s^2	Smoothed value is RMS over the 108-step time arc.
Cross-track accelerations			
biases (2)	5.0×10^{-12} km/s^2	5.0×10^{-12} km/s^2	No improvement (unobservable).
Maneuver ΔV's (12)			
line-of-sight components (12)	1.0×10^{-4} km/s	0.2×10^{-6} km/s	
cross-track components (6)	1.0×10^{-4} km/s	1.0×10^{-4} km/s	Only 6 cross-track (unobservable) ΔV components included.
Satellite positional parameters (19)	400.0 km	50.0 km	RMS of the 19 parameters.
Satellite masses (4)	50.0 km^3/s^2	5.0 km^3/s^2	
Jupiter mass (1)	600.0 km^3/s^2	40.0 km^3/s^2	
Jupiter Ephemeris (3)	400.0 km	200.0 km	
Station Location errors:			3 tracking stations.
spin-axes (3)	1.5 m	0.4 m	
Longitudes (3)	3.0 m	0.5 m	
Range Biases (3)	100.0 km	1.0 km	Range measurement biases, one for each station.
Camera pointing angles (3)			Independent from frame to frame (white)
clock, cone	0.3 deg	1.0×10^{-4}	Smoothed values RMS over 87 frames.
twist	1.0 deg	0.2 deg	

TABLE II
MEASUREMENT MODEL WITH *A POSTERIORI* FIT RESULTS

Data Type	A Priori Uncertainty	Smoothed Estimate RMS residuals	# Data Points
Radiometric:			
Doppler (60 sec. sample average)	1.0 mm/s	0.4 mm/s	2400
Range	1.0 km	0.1 km	27
Optical	0.5 pixels	0.25 pixels	139 stars 101 satellite images

filter performance. Our concerns are illustrated in [11] which summarizes some of the peculiar (and wrong) numerical results that were obtained in premission simulations of the Voyager Jupiter approach using conventional Kalman filter covariance formulations.

The Earth-based radiometric data are processed using a batch sequential, square-root information filter/smoother [1], [2], and [7], and the spacecraft-based optical data are processed with a $U-D$ covariance factorized Kalman filter [2], [6]. The radiometric observation set is much larger than the set of optical observations; for the encounter application reported here the radiometric data consisted of 2400 Doppler and 27 range measurements and the optical data set consisted of 139 stars and 101 satellite images. The data types and associated statistics are summarized in Table II. As is pointed out in [2] the SRIF is computationally more efficient for larger data sets than is the Kalman filter. It is of interest to note that, despite this, when the other ancillary aspects of the problem are included (such as integration of the variational equations and computation of the measurement observables and differential correction estimate partial derivatives), the difference in computational cost (as will be shown in the following paragraphs) turns out to be relatively unimportant.

To give an idea of the computational burden that is involved, consider a typical radiometric SRIF/SRIS solution with 67 state variables (Table I). This model contains only 4 process noise states (line-of-sight acceleration and 3 camera pointing errors); there are 3500 data points and 132 time propagation steps. The problem run on a UNIVAC 1110, in double precision, used 275 CPU s for filtering; smoothed solutions and covariance computation

used 265 CPU s. The entire run scenario including trajectory variational equation integration, observable partials generation, solution mapping, and generation of smoothed residuals used 4320 CPU s. Thus, the filter and smoother portion each involved little more than 6 percent of the CPU time. Two points of note, in regard to these sample run times are as follows.

1) We generally iterate and generate several filter/smoother solution sets for a given nominal trajectory and file of observation partials. Smoothed covariances use the lion's share of the smoother computation and these need only be computed for the last iteration.

2) The program inputs were not configured to minimize filter/smoother CPU requirements.

For this dynamic state configuration optimally arranged smooth code should require less than 25 percent of the CPU time required for the filter phase. The point we are aiming at is that, based on our experience in [11], a conventional Kalman filter covariance formulation would execute in essentially the same amount of CPU time ($\pm$ 15 percent), and evidently the filter CPU cost is small compared with total run CPU time requirements.

As pointed out in [1] the pseudoepoch state formulation model is an evolutionary outgrowth of the least-squares initial condition estimator [3]. If x_j^c represents current time position and velocity differential correction estimates, then the pseudoepoch state x_j^o is defined by the equation

$$x_j^c = \Phi_{xx}(t_j, t_0)x_j + \Phi_{xy}(t_j, t_0)y + \Phi_{xp}(t_j, t_{j-1})p_{j-1}$$

where the components of y are bias parameters and the components of vector p_{j-1} are piecewise constant stochastic model parameters. The transition matrices $\Phi_{xx}(t_j, t_0)$, $\Phi_{xy}(t_j, t_0)$ and

$$\Phi_{xp}(t_j, t_{j-1}) = \Phi_{xx}^{-1}(t_j, t_0)\Phi_{xp}(t_j, t_0) - \Phi_{xx}^{-1}(t_{j-1}, t_0)\Phi_{xp}(t_{j-1}, t_0)$$

are obtained by integrating variational differential equations for

$$\left[\Phi_{xx}(t, t_0), \Phi_{xy}(t, t_0), \Phi_{xp}(t, t_0)\right]$$

from an epoch time t_0. In Table I the filter state vector x, y, and p components are defined.

Orbit determination problems with radiometric data are ill-conditioned. This is due, in the main, to poor observability, and large dynamic ranges of the variables that are involved (viz. acceleration errors $\sim 10^{-12}$ km/s^2, range values $\sim 10^8$ km, etc). The observability problem is aggravated by the inclusion of large numbers of parameters (such as ephemerides) that are very weakly coupled to the spacecraft observables. The two features of the SRIF/SRIS algorithmic formulation that are most important for this application are as follows.

1) *Numerical reliability:* The SRIF/SRIS algorithms are the most (numerically) accurate and reliable formulation of the Kalman filter/smoother known. Because of the complexity and difficulty inherent in the formulation of the deep space navigation problem it is most important that the estimates and covariances be computed correctly.

2) *Computational efficiency:* The algorithms are formulated so as to exploit the structure of the orbit determination problem. In particular, there are many measurements to be processed per time propagation step, the dynamical model involves only a small number of stochastic variables, there are a preponderance of bias parameters, and the position-velocity states are cast in a pseudoepoch state formulation. Early tests demonstrated that the SRIF, for this structure, was more efficient than a conventional (and less reliable) Kalman filter mechanization.

Using the SRIF it is relatively easy to take the processed results and generate estimates that correspond to models with a smaller number of bias parameters. This feature is especially useful for confirming that parameters thought to be of little significance turn out, in fact, to have little effect on the key estimate state vector components.

The $U-D$ covariance factorization was chosen to mechanize the optical navigation filter for many of the same reasons (numerical reliability and computational efficiency), except in this case the measurement set per time propagation is small, and for such problems the $U-D$ formulation is more efficient than the SRIF. In [11] the $U-D$ formulation and the Kalman filter both conventional (optimal) and stabilized (Joseph/suboptimal) forms are compared for a Jupiter approach simulation with radiometric data. In the tests reported there the covariance mechanized filters performed very poorly; they gave results that ranged from inaccurate, but which might be thought correct (20–50 percent errors) to impossible (negative variances and estimates that were absurd). It happens that optical navigation data are not nearly as ill-conditioned as are the radiometric data, and in fact, the early optical navigation studies successfully carried out in [5] used a conventional Kalman filter mechanization. The decision to use a $U-D$ factorization in place of the conventional mechanization was based on the following facts:

1) Comparisons (operation counts, actual CPU, and storage requirements) show that *optimally coded* $U-D$ and conventional covariance mechanizations are nearly indistinguishable in terms of storage and computational requirements.

2) $U-D$ factor mechanization has accuracy that is comparable with the SRIF. On the other hand, one cannot be certain when the covariance mechanization will degrade or fail (e.g., when the *a priori* uncertainties are too large, the measurement uncertainties are too small, the data geometry is near linearly dependent, etc., one can expect stability and accuracy problems).

It is the conviction of (one of) the authors (who is believed by the others!) that covariance mechanized Kalman filters should *never* be computer implemented. Further, it is believed that if the Kalman filter applications community had more experience with efficiently and reliably mechanized factorization alternatives, there would be few instances where a covariance mechanized Kalman filter would find application. We note in closing this factoriza-

TABLE III
SUMMARY OF JUPITER APPROACH ORBIT CONTROL

Voyager 1 TCM	Execution Time	ΔV, m/sec Designed	ΔV, m/sec Achieved	ΔB̄, Km ΔB·R	ΔB̄, Km B·T	ΔT
3	E - 35 days	4.146	4.208	-1725.	+13125.	$+0^h\ 14^m$
4	E - 12.5 days	0.586	0.594	+710.	-100.	$-0^h\ 0^m\ 14^s$
Voyager 2 TCM						
3	E - 45 days	1.442	1.384	+3330.	+5040.	$-0^h\ 4^m\ 42^s$
4	E - 12 days	0.576	0.574	-895.	+210.	$+0^h\ 0^m\ 03^s$

tion algorithm discussion that the SRIF and $U-D$ algorithms that were used in this application have been refined and generalized, and are commercially available in the form of portable Fortran subroutines [12].

III. OD Performance

This section will summarize the near-encounter OD results for both spacecraft. These results are 1) the orbit determination that was done to deliver the Voyager spacecraft to their required final target points met the required accuracies; and 2) that the final postdelivery orbit determination needed to accurately point science instruments in the near and postencounter phases also exceeded specification accuracies. A limitation of the Voyager orbit determination program is that one can include at most 70 filter states, and this includes the sum of both estimated and consider filter states. For completeness we remind the reader that consider parameters, cf. [1] and [2], play no role in the estimation except to provide a deweighting to the confidence one would otherwise put on the estimates. As noted earlier, the size limitation does not allow us to include all the known error sources in the filter model. Table I lists one of the several filter models that were used, and quantifies the results obtained. Observe that although there are 12 maneuvers only six cross-track maneuver correction terms are included, and these terms have a negligible effect on estimator performance. This conclusion is based both on estimate comparisons with and without such terms included and on the incremental change in the computed covariance due to the addition of consider parameter sensitivity effects. The discussion that follows is an elaboration of the results summarized in Table I.

Jupiter Approach Solutions

For approximately the last 60 days of each approach, both radio and optical data were continuously acquired to allow orbit estimates to be revised every few days. Optical data in the time period beginning 60 days from encounter (E) to $E-30$ days were acquired at the rate of approximately one picture per day, and this rate increased to about four or five pictures per day in the last few days before encounter. Radio tracking (coherent Doppler and range) was virtually continuous for the last 60 days of approach. For each encounter, there were several critical events for which orbit estimate deliveries to certain elements of the project were required. The events consisted of two trajectory correction maneuvers, at about $E-40$ days and $E-12$ days, and several updates to the onboard instrument pointing, a critical element in the near encounter science return. The detailed summary of the delivery events for each spacecraft is shown in Table III.

Based on a preliminary data acquisition schedule, covariance analysis estimates were computed preflight of the orbit determination errors which would result at these various delivery times. The primary purpose of this section is to compare the near real-time filter and the current best reconstructed smoothed orbit estimates, and also to compare both of these to the expected covariance performance computed preflight. It will be shown that all orbit estimates but one fell well within the expected preflight capability ($1-\sigma$) even though those early statistics were derived with unrealistic, very optimistic, assumptions about the "small" nongravitational forces caused by spacecraft attitude changes.

More specifically, as discussed in Section II, the spacecraft's attitude control system did not employ coupled thrusters, and hence there were many small velocity impulses imparted to the spacecraft. These velocity impulses are impossible to model individually, and affect (to a sensible level) the meter level ranging and submillimeter/second Doppler observables if they are imparted along the Earth-line. In addition, whenever the spacecraft orientation was changed to allow an engineering calibration, or a science scan of the Jovian system, velocity impulses of tens of millimeters per second were imparted. These larger impulses were not accounted for in the preflight analysis, and the more continuous smaller impulses resulted effectively in accelerations of the order of $5-10\times10^{-12}$ km/s^2 along all three spacecraft axes. The larger impulsive velocity changes have two effects. When they occur within the data arc, an estimate of their components becomes confused with the estimates of the dynamically important parameters, and the result is an incorrect orbit; when they occur past the end of the data arc they cause incorrect mapping to the encounter time, and the result is an incorrect prediction of encounter conditions. Based on covari-

ance analyses, it did not appear possible to accurately predict the velocity components at the maneuver event times from *a priori* information.

Data Weighting

In the vicinity of a planetary encounter, the radio and optical data are geometrically complementary. The Earth-spacecraft line-of-sight range and velocity measurements indirectly provide the spacecraft-planet distance through observable dynamic effects, and the optical data effectively measure the instantaneous spacecraft-satellite cross line-of-sight position relative to a particular satellite. The radio and optical data were planned to allow determination of both the satellite orbits and the spacecraft trajectory relative to the planet.

In the estimation process using both radio and optical observations, the solutions at certain stages were found to be sensitive to the relative weighting of the two data types. Based on the image extraction analysis, the optical data were thought to measure the star and satellite center locations to 0.5 pixels or less in a random measurement noise sense. In addition, if there were any systematic optical image extraction errors, they were thought to be small (< 0.5 pixels) and to behave as biases in the 2-D picture space, or as long term slowly varying functions, i.e., nearly biases. Using these arguments the optical data usually were assumed to have 0.5 pixel measurement noise; 0.5 pixel optical biases were used as consider parameters to compute the expected uncertainty in the orbit estimates. Incidentally, these two consider parameters, together with the 67 estimated parameters listed in Table I, essentially exhausts the 70 parameter ODP storage limitation.

After calibrating for troposphere, ionosphere, and space plasma effects, the measurement errors for radio data are equivalent to only a few meters in range and 0.3–0.5 mm/s for a 60 s count time for Doppler. However, because of the known level of unmodelable nongravitational accelerations, range was more usually weighted at 100 m, and Doppler at 1 mm/s, for a 60 s count time. These values, together with the postfit rms residual results are displayed in Table II. For the radio data, the most likely sources of error are transmission media calibration errors and Earth station location errors, both of which are usually combined into an assumed systematic error with a diurnal signature. Data noise for Voyager 2 was larger because its view periods occurred during local daylight hours, when transmission media effects were larger. The Voyager 2 encounter also coincides with a more active solar period.

Reconstruction of Encounter Orbits

Since the encounters, it has been possible to do a detailed analysis of the larger nongravitational impulsive events for Voyager 1, using data from approximately 60 days after encounter. In addition to errors associated with the two-approach TCM's, there occurred 10 preencounter events whose effects were directly observable along the Earth-line and which therefore were estimated as impulsive

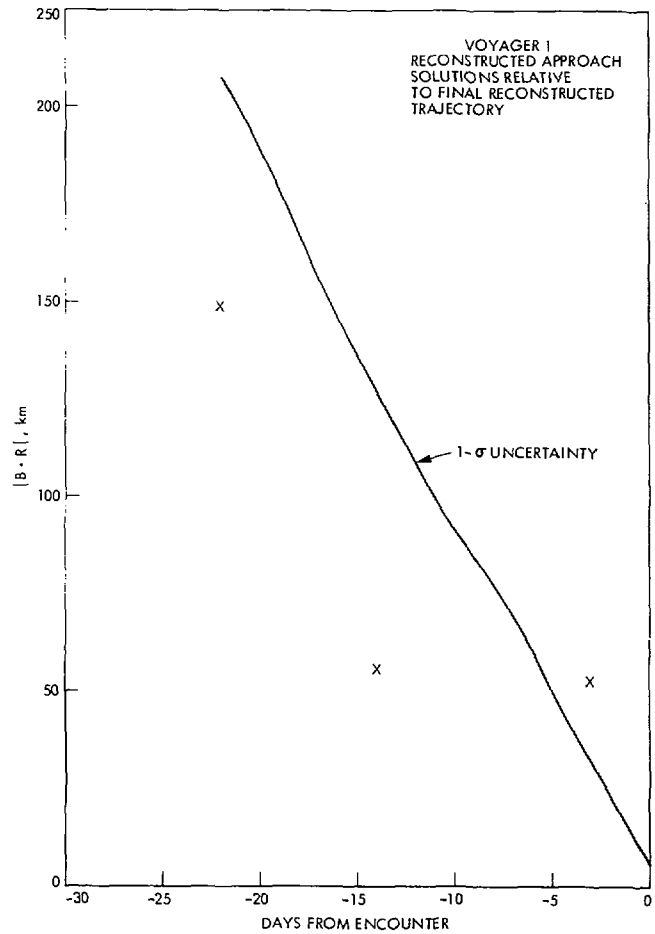

Fig. 5. Reconstructed history of Voyager 1 $B \cdot R$ solutions relative to postencounter reconstructed orbit.

ΔVs; these are the $12\Delta V$ state vector components included in Table I.

One of the best ways to measure the real limit to the orbit determination capability as a function of time to encounter is to examine the variation in solutions along a trajectory which has already passed through several estimation iterations for the magnitude of the impulsive components. With as detailed a treatment of the larger impulsive events as is possible, and with stochastic and constant acceleration components solved for in the sequential filter to remove any excess nongravitational effects, the relative time history B-plane[1] solutions for the last 25 days before Voyager 1 encounter were computed and are displayed in Figs. 5 and 6 along with the $1-\sigma$ uncertainties in these solutions. These uncertainties were calculated using no assumed systematic errors in either radio or optical data, such as optical biases, and therefore represent lower limits to the error that could be expected. In general, the solutions fall within even this optimistic uncertainty level. The 55 km $\Delta B \cdot R$ solution at $E - 3.5$ days is the only anomaly

[1]Planetary targeting is usually expressed in terms of the *B-plane*, a plane passing through the center of a target planet and perpendicular to the incoming approach hyperbola asymptote of a spacecraft. "$B \cdot T$" is the intersection of the B-plane with the ecliptic and "$B \cdot R$" is a vector in the B-plane that is perpendicular to $B \cdot T$ and making a right-handed system R, S, T, where S is the incoming asymptote.

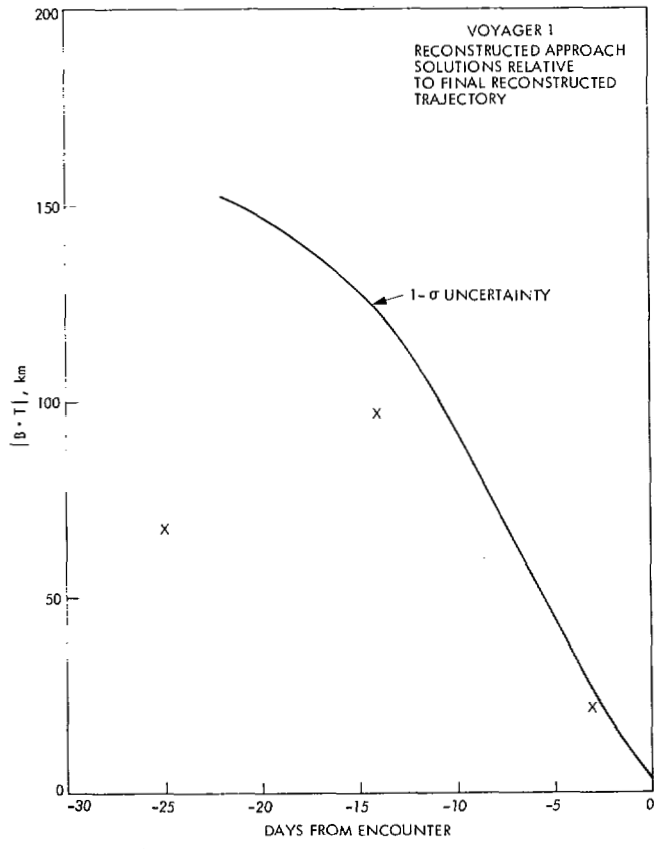

Fig. 6. Reconstructed history of Voyager 1 $B \cdot T$ solutions relative to postencounter reconstructed orbit.

and it occurs at a time when significant ($>1-\sigma$) transients are occurring in several important dynamic parameter estimate components, such as, for example, planet mass. Significant parameter estimate variations in static components such as this indicate possibly a station location, media, or nongravitational mismodeling problem. The behavior in the $B \cdot R$ estimate also suggests the possibility of an optical center-finding error which would become significant only when the satellite diameters in the picture become very large (approximately 100 pixels). However, an analysis of the center-finding at this time period for all the different satellites indicates that this is an unlikely possibility. A center finding error would also imply that earlier satellite residuals would show strong systematic effects. This was not, however, observed when the entire arc of optical residuals was plotted from the current best reconstruction run. (The orientation of the Voyager camera in space was such that to within about 20°, pixels represent a measurement in the ecliptic or trajectory plane, and lines represent measurements that are normal to this plane.)

A slight slope in the smoothed estimate line residuals seems to indicate that there is some remaining out-of-trajectory-plane mismodeling, but the error at encounter caused by this slope should be no more than 10–15 km. This same error behavior was observed to occur in the near-real time approach solutions. The general results and conclusions stated here were derived mostly from the Voyager 1 orbit reconstruction experience; they are applicable directly, however, to Voyager 2.

Real-Time Solutions

In this subsection we compare the near-real time trajectory estimates for both spacecraft that were delivered to the Voyager project at certain stages of each approach, to the final reconstruction solutions, and compare the accuracies of these deliveries to the attainable accuracies.

The Voyager 1 approach solutions relative to reconstruction are shown in Figs. 7 and 8. The lump, or flattening, in the Voyager 1 uncertainty curves reflects the fact that the data arc for this and subsequent solutions was shortened to include data only within 30 days of encounter. In general, near-real time orbit determination accuracies for both spacecraft fell well within the $1-\sigma$ uncertainties, which are taken from the computer run that was made in near-real time. The errors (with smoothed estimates regarded as truth) also generally fell well within the preflight covariance predictions. The only point on approach at which the near-real time solutions were not substantially below the $1-\sigma$ uncertainty level occurred on Voyager 1 at the final delivery for the last approach trajectory correction maneuver TCM4. After considerable study it became apparent that the relative weighting of the radio and optical data at this epoch was responsible for this anomalous estimate.

The variability of the Voyager 1 B-plane solutions leading up to the final TCM4 delivery at $E-15$ days are shown in Figs. 9 and 10 as functions of time, relative data weightings, and estimated parameter list. The correct (best postfit) answers are indicated in each figure. The solutions plotted by the small circles in Fig. 9 were generated by solving for the state vector whose components are listed in Table I; the estimate list includes spacecraft state, stochastic and constant nongravitational accelerations, several impulsive ΔVs, planet mass, and planet and satellite ephemerides, as well as the three camera orientation angles, which were always estimated. The solutions of Fig. 10 also included Earth station locations in the estimate list. In both figures there are significant sensitivities for all three curves to both data arc length and relative radio/optical weightings. Comparison of the results of Figs. 9 and 10 indicates that there is a large sensitivity (of the order of several hundred kilometers for the radio only case) to station location, or station location-like, errors. This type of sensitivity typically is an indication of mismodeling of the radio observables.

The orbit determination performance for the last approach TCM and the pointing update for Voyager 2 are summarized in Fig. 11 in which the B-plane conditions predicted using data to $E-17$ days and $E-9.5$ days and their uncertainty ellipses are compared to the final reconstruction orbit estimate. Because of the Voyager 1 experience and because of the difficulty encountered with a long arc of Voyager 2 radio data, many different arc lengths and combinations of data and parameter estimate lists were used for the second spacecraft. By thus experimenting we were able to eliminate the larger effect of systematic mismodeling and arrived at solutions that fell well within all of the uncertainty ellipses.

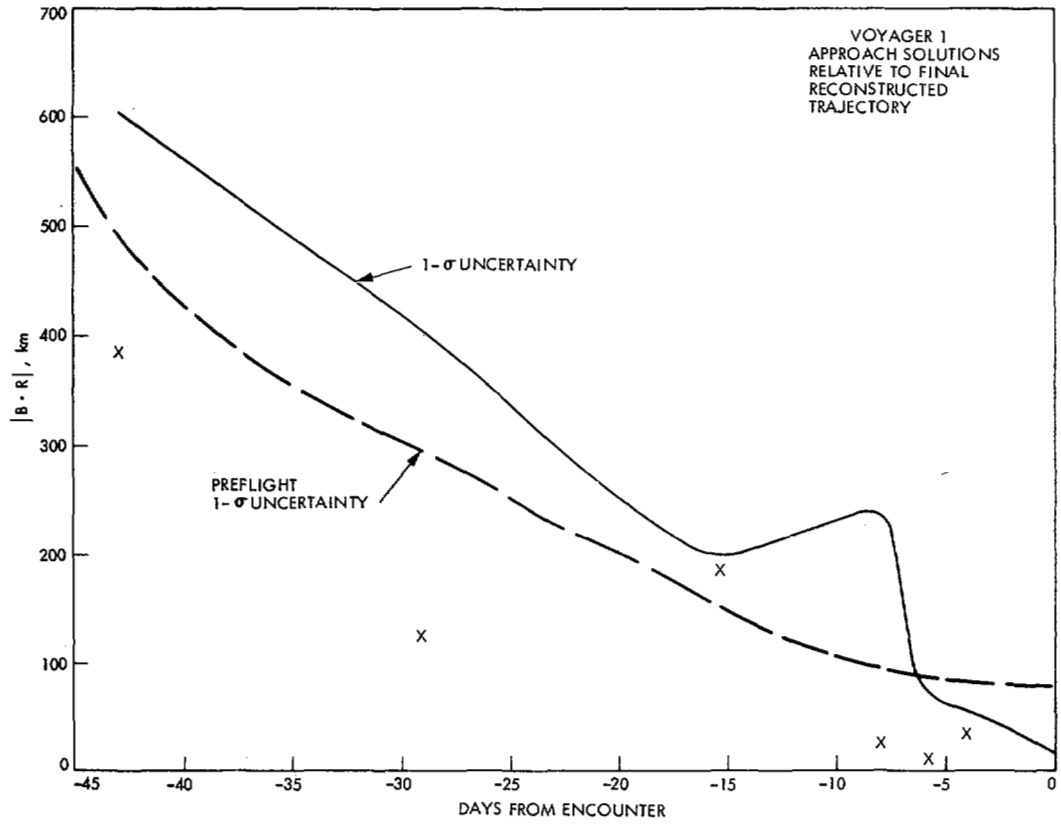

Fig. 7. History of Voyager 1 real-time $B \cdot R$ solutions relative to postencounter reconstructed orbit.

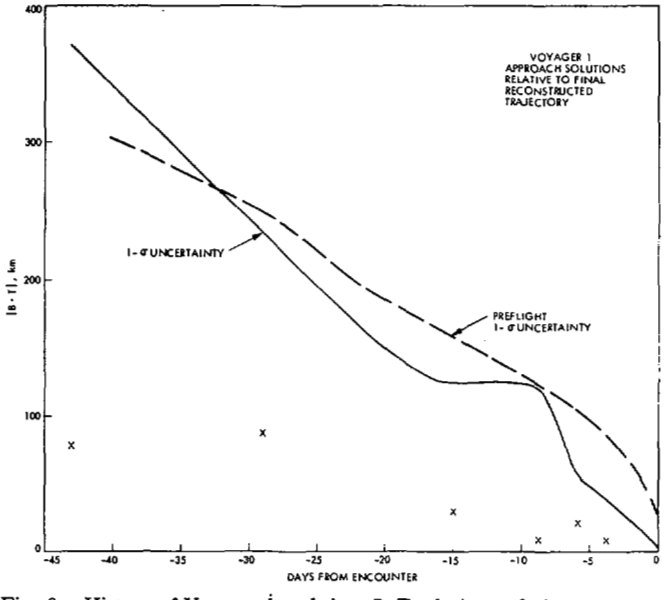

Fig. 8. History of Voyager 1 real-time $B \cdot T$ solutions relative to postencounter reconstructed orbit.

IV. Summary of OD Performance

Tables IV and V indicate the OD delivery performance for each spacecraft. The last columns of each table show that the delivery OD performance for each spacecraft easily met the established accuracy criteria. In the case of Voyager 2, the delivery requirements were less stringent, and the achieved delivery was nearly equivalent to 0.5 pixel, Jupiter relative. Figs. 12 and 13 give a brief indication of the overall capability and performance of the Voyager radiometric data. Fig. 12 shows, in geocentric angular coordinates, the shift in Jupiter position coordinates obtained from a set of orbit estimates based on radiometric data arcs extending from $E-60$ to $E+30$ days. This data arc allows for an accurate Jupiter-relative orbit estimate and some sensitivity to Jupiter ephemeris error. One solution estimates only ephemeris error; the second solution estimates both ephemeris and station location errors, and essentially trades off these two error sources to give the same net geocentric angular offset as the ephemeris-only solution. This plot indicates the general inability of Earth-based radiometric data to fully distinguish station location error from ephemeris error, and sets a lower bound of about 0.25 μrad to the Voyager radiometric performance. Fig. 13 plots in geocentric angular coordinates the radio-based OD that was done for the final Voyager 1 delivery, and compares this real-time result with the best reconstructed orbit at the delivery point, obtained using a combined radio plus optical data set. This plot shows that the radiometric OD for Voyager 1 performed to about the 0.5 μrad level.

V. Satellite State Estimates

A natural fallout of using the optical and radio data in the spacecraft trajectory determination process is the improvement in the knowledge of the orbits of the four Galilean satellites. The optical data are directly sensitive to satellite position changes. Near the satellite close ap-

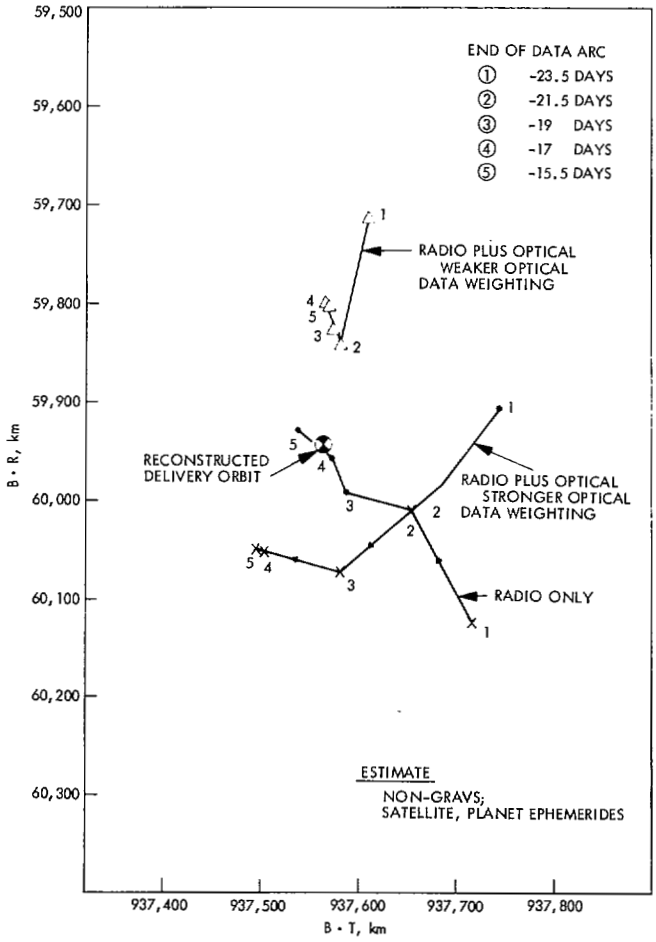

Fig. 9. Variation in Voyager 1 real-time *B*-plane solutions; station locations not estimated.

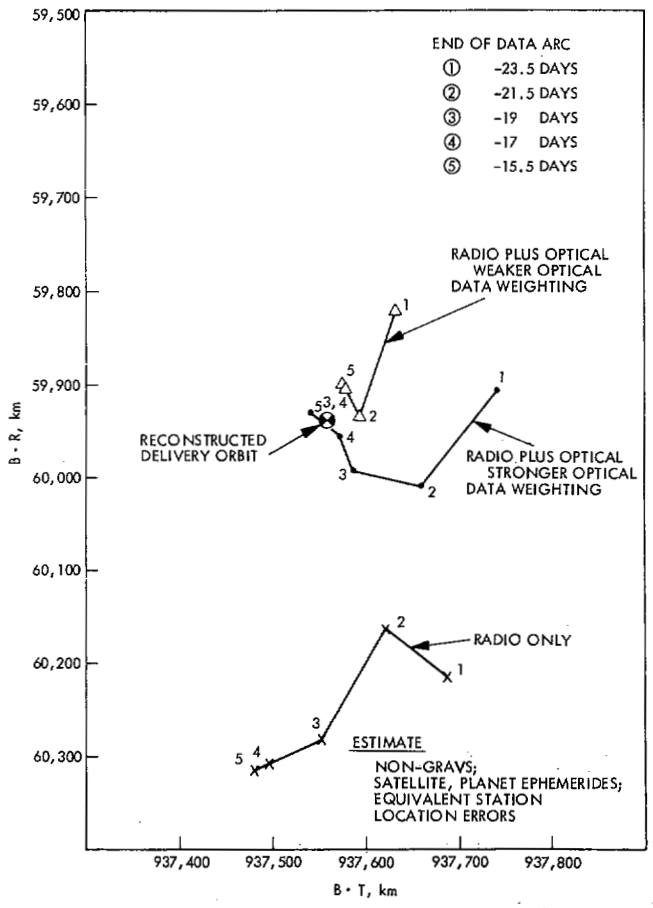

Fig. 10. Variation in Voyager 1 real-time *B*-plane solutions; station locations estimated.

proaches, the radio data are sensitive normal to the line-of-sight to the dynamic effects on spacecraft motion due to satellite mass or position errors in certain directions. The combination of both data types from both Voyager encounters results in a Galilean satellite ephemeris significantly improved over that available to Voyager from Earth-based observations [15]. A brief summary of the orbit estimates based on the Voyager 1 data is briefly discussed here.

A dynamical theory for the Galilean satellites developed by Lieske [13], [14] was used to compute both residuals and partials for the optical data and to develop the ephemerides which were the starting point for the Voyager analyses. The adjustable Lieske parameters (included as satellite positional errors in Table I) consist of three constants for each satellite which are fractional errors in the mean motion, the eccentricity and the sine of the inclination and three angular parameters which are essentially the initial longitude, the argument of periapse, and the nodal position. The changes to the estimated Lieske parameters, and the *a priori* and *a posteriori* errors for these parameters are shown in Table VI. In addition, the masses of the satellites, and Jupiter, and the right ascension and declination of the north pole of Jupiter are also adjustable.

In the analysis described here the arguments of periapse were not estimated because their effect on the data was

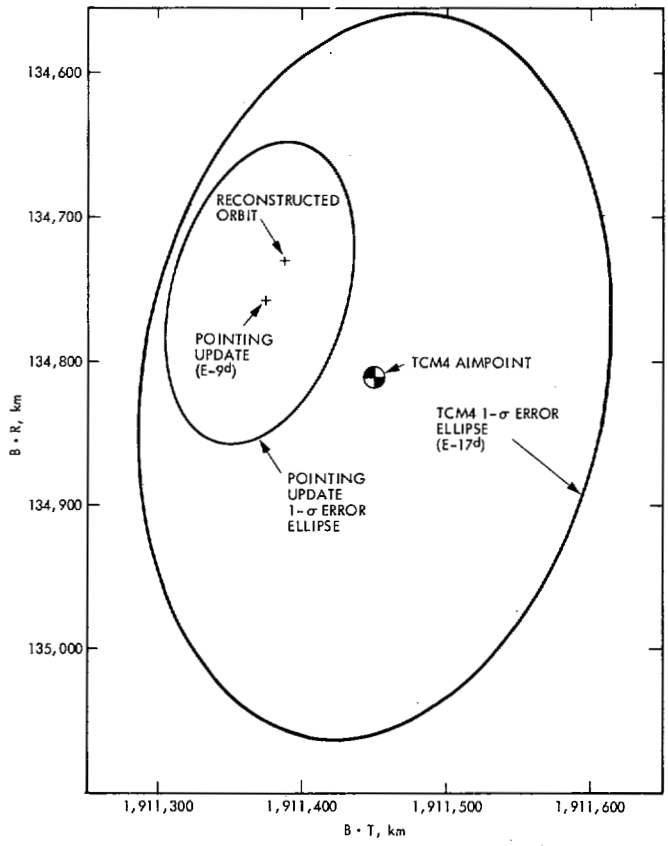

Fig. 11. Voyager 2 approach OD performance.

TABLE IV
SUMMARY OF VOYAGER 1 NAVIGATION DELIVERY PERFORMANCE

Control Parameter	Rationale	Target Value	Achieved Value	Allowable Error	Actual Error
Geocentric occulation entry	Timing of Jupiter limb scan at occulation	March 5, 1979 15:45:20.7	March 5, 1979 15:45:22.1	30 sec	+1.4 sec
Distance off center-line of flux tube model, km	Guarantee sampling of current in Io flux tube	-7.4 km	+101 km	1000 km	108 km
Io closest approach time	Io mosaicking sequence control	March 5, 1979 15:13:18.9	March 5, 1979 15:13:20.7	20 sec	+1.8 sec

Final delivery maneuver was executed 12.5 days prior to Jupiter closest approach.

TABLE V
SUMMARY OF VOYAGER 2 NAVIGATION DELIVERY PERFORMANCE

Control Parameter	Rationale	Target Value	Achieved Value	Expected 1-σ Performance	Actual Error
Jupiter B-plane coordinates	Minimize magnitude of post-Jupiter TCM5	B.R = 134,804 km B.T = 1,911,454 km	134,730 km 1,911,387 km	220 km 161 km	-74 km -67 km
Jupiter closest approach time	Pointing control of Earthline TCM5	7/9/79 $22^h29^m0^s$ GMT	7/9/79 $22^h29^m1.6^s$ GMT	22 sec	+1.6 sec

Final delivery maneuver was executed 12 days prior to Jupiter closest approach.

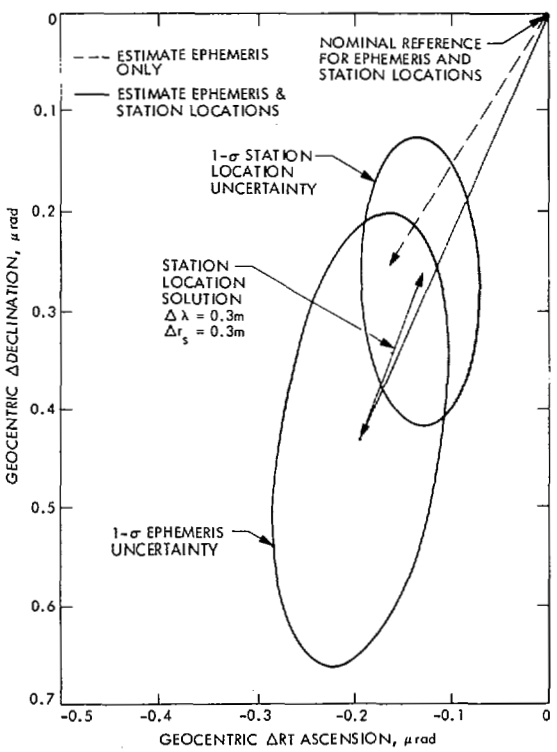

Fig. 12. Indication of Voyager 1 radiometric capability.

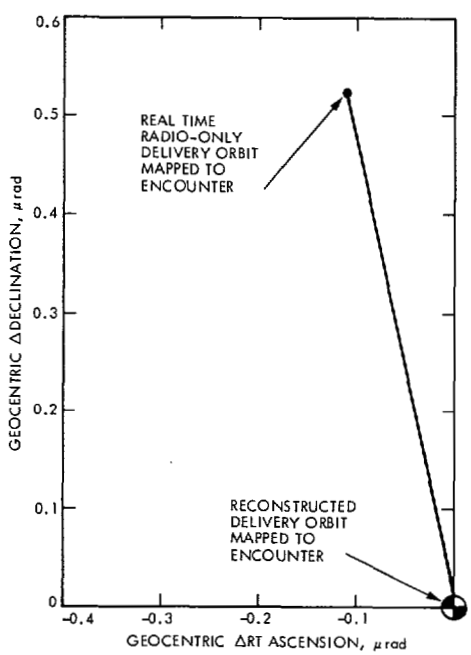

Fig. 13. Voyager 1 radiometric performance at delivery.

known to be small (less than about 15 km). Mean motions, whose values were extremely well-determined from many years of Earth-based data were also not included.

A comparison of the formal standard errors in Cartesian coordinates determined from the Earth-based and Voyager 1 data (using the Earth-based estimates as *a priori*) is shown in Table VII in which the entries represent the RSS of the sigmas and the changes in the three components of position of each satellite at the epoch of Voyager 1 Jupiter closest approach. The Voyager 1 *a posteriori* errors are very similar for all the satellites with the slight differences explainable by the variability of optical data distribution and quantity, and by the ratio of the satellite periods which affects the "average quality" of the data around the observed orbits. The Cartesian changes at the encounter

TABLE VI
CHANGES TO ESTIMATED LIESKE PARAMETERS

	Lieske Parameter	Δ	a posteriori σ	Earth-based a priori σ
	5EPS 16	-.175	.213	.42
	5EPS 17	-.0022	.179	.26
eccentricity	5EPS 18	-.013	.0071	.019
	5EPS 19	.0024	.0013	.0036
	5EPS 21	-.134	.174	.41
	5EPS 22	-.0082	.0066	.025
sine i	5EPS 23	.0032	.020	.050
	5EPS 24	-.0114	.018	.11
	5BET 01	-.0014	.0028	.017
long	5BET 02	-.0045	.0011	.004
	5BET 04	-.0054	.0005	.005
	5BET 11	7.5	5.7	18.0
node	5BET 12	.512	.575	1.05
	5BET 13	.407	1.16	2.5
	5BET 14	-.551	.817	2.4
pole RA	ZACPL 5	.0064	.0084	.05
pole DEC	ZDEPL 5	-.0003	.0049	.026
Satellite, Jupiter masses	501 GM	29.4	4.6	56
	503 GM	3.6	3.5	76
	504 GM	7.5	1.4	47
	GM 5	657.5	24.7	1200

TABLE VII
COMPARISON OF CARTESIAN FORMAL STANDARD ERRORS AND CORRECTIONS

	Earth Based a priori σ	Voyager a posteriori σ	Voyager Δ (RSS)
Io	87	28	35
Europa	137	28	43
Ganymede	161	34	80
Callisto	448	35	180

Computed from Voyager 1 Encounter Data.
Numbers shown are RSS of x, y, z components.
Epoch of Corrections = March 5, 1979 12:05 GMT

epoch are well within the Earth-based *a priori*, but may vary somewhat at other points of the orbit. Only changes to the longitudes of Europa and Callisto were of the order of an *a priori* sigma. It is apparent that the *a priori* ephemeris was an excellent product.

VI. CONCLUSIONS

We have shown that the orbit determination performed to deliver each spacecraft to its target at Jupiter was within the predicted capability of the radiometric and optical-based navigation system for Voyager, and in fact improved for Voyager 2 as a result of the Voyager 1 experience. The postdelivery OD knowledge solutions done to refine scan platform pointing were well within the stated requirement, even though the knowledge epochs were earlier than anticipated prelaunch.

Numerous tests were made throughout the mission to test estimate consistency and accuracy of the SRIF/SRIS and $U-D$ algorithm implementations. The navigation estimation software performed flawlessly. Indeed, the estimation software performed so well that most of the time it was taken for granted by the navigation team, and that is the ultimate compliment.

As a result of having actually used satellite images to perform Jupiter and satellite-relative navigation, it has been determined that several prelaunch hypotheses regarding error sources for optical measurements were not correct. Specifically, before the encounter experience it was assumed that center-finding errors for large satellite images would scale with the size of the image. From a detailed analysis of hundreds of images it was found that the center finding errors were more likely to either decrease with increasing image size, or to remain essentially constant. As indicated in Table II the rms noise associated with the optical measurement postfit residuals were found to be about 0.25 pixel as compared with the 1.0 pixel error assumed prelaunch. It is to be expected that the postfit residuals should have a smaller rms than the data noise σ because it is known that the postfit residual $z_j - Hx_{j:n}$ has variance

$$\sigma^2 - HP_{j:n}H^T.$$

In addition, we have learned that the combination of radiometric with optical measurements must be done carefully, with regard to the information content of each data type. This was especially true in the case of Voyager, which represented a distinct extreme in the level of dynamical corruption of the radiometric signal by small spacecraft-generated velocity pulses, that did not affect the corresponding optical data.

ACKNOWLEDGMENT

J. E. Reidel provided much of the postencounter computer support for this paper.

REFERENCES

[1] G. J. Bierman, "Sequential least-squares using orthogonal transformations," Jet Propulsion Lab., Pasadena, CA, Aug. 1, 1975, Tech. Memorandum 33-735.

[2] G. J. Bierman, *Factorization Methods For Discrete Sequential Estimation*. New York: Academic, 1977.

[3] T. D. Moyer, "Mathematical formulation of the double-precision orbit determination program (DPODP)," Jet Propulsion Lab., Pasadena, CA, May 15, 1971, Tech. Rep. 32-1527.

[4] J. Ellis, "Voyager software requirements document for the orbit determination program (ODP) Jupiter encounter version," Jet Propulsion Lab., Pasadena, CA, May 10, 1977, Rep. 618-772.

[5] N. Jerath, "Interplanetary approach optical navigation with applications," Jet Propulsion Lab., Pasadena, CA, June 1, 1978, Pub. 78-40.

[6] S. P. Synnott, "Voyager software requirements document," Jet Propulsion Lab., Pasadena, CA, July 10, 1977, Pub. 618-729.

[7] G. J. Bierman, "Square-root information filtering and smoothing for precision orbit determination," *Mathematical Programming Study 18, Algorithms and Theory in Filtering and Control*, 1982, pp. 61–75.

[8] J. K. Campbell, S. P. Synnott, J. E. Reidel, S. Mandel, L. A. Morabito, and G. C. Rinker, "Voyager 1 and Voyager 2 Jupiter encounter orbit determination," presented at the AIAA 18th Aerospace Sci. Meet., Pasadena, CA, Jan. 14–16, 1980, paper AIAA 80 0241.

[9] C. S. Christensen, "Performance of the square-root information filter for navigation of the Mariner 10 spacecraft," Jet Propulsion Lab., Pasadena, CA, Jan. 1976, Tech. Memorandum 33-757.

[10] J. K. Cambell, R. A. Jacobson, J. E. Reidel, S. P. Synnott, and A. H. Taylor, "Voyager I and Voyager II Saturn encounters," presented at the 20th Aerospace Sci. Meet., Jan. 1982, paper AIAA 8-82-0419.

[11] G. J. Bierman and C. L. Thornton, "Numerical comparison of Kalman filter algorithms; Orbit determination case study," *Automatica*, vol. 13, pp. 23–35, 1977.

[12] G. J. Bierman and K. H. Bierman, "Estimation subroutine library, directory and preliminary user's guide," Factorized Estimation Applications, Inc., Sept. 1982.

[13] J. H. Lieske, "Improved ephemeris of the Galilean satellites," *Astrophysics*, vol. 82, pp. 340–348, 1980.

[14] J. H. Lieske, "Theory of motion of the Galilean satellites," *Astron. and Astrophys.*, vol. 56, pp. 333–352, 1977.

[15] S. P. Synnott and J. K. Campbell, "Orbits and masses of the Jovian system from Voyager data: Preliminary," presented at the IAU-Colloquium 57, Institute for Astronomy, Univ. Hawaii, May 1980.

James K. Campbell was born in Brooklyn, NY, on July 1, 1942. He received the B.S. and M.S. degrees from the School of Engineering, University of California, Los Angeles, in 1964 and 1966, respectively.

He has worked at the Jet Propulsion Laboratory, California Institute of Technology, Pasadena, since 1966. He contributed to the encounter trajectory design of the Mariner 6 and 7 missions to Mars and the Pioneer 10 and 11 missions to Jupiter, and to the orbit determination analysis for the Viking missions to Mars. Most recently, he participated in the navigation of the Voyager spacecrafts to Jupiter and Saturn as leader of the Orbit Determination Group.

Mr. Campbell is a member of the American Geophysical Union and the American Institute of Aeronautics and Astronautics.

Stephen P. Synnott was born in NJ in 1946. He received the B.S. degree in aeronautical engineering from Rensselaer Polytechnic Institute, Troy, NY, in 1968 and the M.S. and Ph.D. degrees in astrodynamics from Massachusetts Institute of Technology, Cambridge, in 1970 and 1974, respectively.

Since 1975 he has been employed at the Jet Propulsion Laboratory, California Institute of Technology, Pasadena, where he specializes in spacecraft navigation, image processing, and celestial mechanics.

Gerald J. Bierman (M'68–SM'77) received the Ph.D. degree in applied mathematics from the Polytechnic Institute of New York, Brooklyn, NY, in 1967, and the M.S. degrees in electrical engineering and mathematics from the Courant Institute and School of Engineering, New York University, New York, respectively.

He worked at Litton Systems Guidance and Controls Division, developing and analyzing suboptimal Kalman filter designs, and at the Jet Propulsion Laboratory, California Institute of Technology, Pasadena, where he was responsible for creating high precision orbit determination and reliable parameter estimation software. In 1979 he served as a NATO consultant and soon after created *Factorized Estimation Applications*, a small consulting firm specializing in high-quality numerically reliable estimation software. He is known for his contributions related to the square-root information filter/smoother and the $U-D$ covariance factorized Kalman filter. He has considerable navigation system applications experience, over fifty refereed publications, and a research monograph, *Factorization Methods for Discrete Sequential Estimation* (New York: Academic, 1977) that is devoted to the computational aspects of estimation. His publications and applications experiences have sensitized both estimation researchers and control applications engineers to the importance of estimation algorithms that are both efficient and numerically reliable.